PHYSICAL REVIEW B VOLUME 20, NUMBER 11 1 DECEMBER 1979

# Amorphous to crystalline transformation of $Fe_{80}B_{20}$

A. S. Schaafsma, H. Snijders, and F. van der Woude
*Solid State Physics Laboratory, Materials Science Center, University of Groningen, Groningen, The Netherlands*

J. W. Drijver and S. Radelaar
*Department of Technical Physics, University of Utrecht, P. O. Box 80000, Utrecht, The Netherlands*

(Received 11 May 1979)

The transformation from the as-quenched amorphous to the crystalline state of $Fe_{80}B_{20}$ was followed isothermally at relatively low temperatures (580 to 630 K) with Mössbauer-effect spectroscopy (MES). Both the Allied Chemical Metglas 2605 $Fe_{80}B_{20}$ and twin-roller quenched (RQ) $Fe_{80}B_{20}$ were studied. Before the onset of crystallization the Mössbauer recoil-free fraction of the $^{57}Fe$ nuclei was constant but it increased by about 15% during crystallization. This implies that on the average the Fe atoms are more firmly bound in the crystalline than in the amorphous state. From a combination of MES, x-ray diffraction, and optical microscopy it was found that (a) the MG 2605 ribbons are rather inhomogeneous in the sense that 10% to 15% of the ribbon cross section is considerably more resistant to crystallization than the remaining part, (b) no such inhomogeneity is present in the RQ ribbons, (c) the crystallization takes place by the eutectic type of reaction, the crystallization products are $\alpha$-Fe and the (metastable) tetragonal $Fe_3B$ compound, and (d) a quantitative analysis of the kinetics of the transformation suggests that crystallization occurs only by the growth of (crystalline) nuclei which are already present in the as-quenched amorphous material.

## I. INTRODUCTION

Metallic glasses are usually assumed to be structurally and chemically homogeneous as a result of the very high rate of quenching from the liquid state. But it is also known that the structure of the glass depends on the quenching conditions and on the subsequent thermal history. For example, the mechanical properties and the stability of metallic glasses can be changed significantly by changing the effective quenching rate. This was observed by Chen and Polk[1] and Chi *et al.*[2] for Fe-based alloys and by Lewis and Davies[3] for Pd-Si alloys. Also, upon annealing of the as-quenched material at relatively low temperatures, mechanical[4] and magnetic[5] properties change before crystallization sets in. During this process of structural relaxation Egami[6] recently found small changes in the x-ray structure factor of Metglas $Fe_{40}Ni_{40}P_{14}B_6$.

Thus it is well established that the structure of a metallic glass is not too well defined. The as-quenched structure depends on the quenching conditions and can be changed by a subsequent anneal at sufficiently low temperature without the interference of crystallization.

In the present paper the (micron scale) homogeneity of the as-quenched amorphous state and the kinetics of the transformation to the crystalline state of the metallic glass $Fe_{80}B_{20}$ are studied. We compared commercially available $Fe_{80}B_{20}$ (Allied Chemical Metglas 2605), which is quenched by a one-substrate technique, with $Fe_{80}B_{20}$ quenched with the twin-roller, two-substrate technique.[7] The amorphous to crystalline transformation was followed at relatively low temperatures using the Mössbauer-effect technique with $^{57}Fe$ as the Mössbauer isotope. The temperatures were chosen in such a way that the time required for the complete transformation ranged from about 10 hours to a few weeks. The time needed to collect a Mössbauer spectrum with fair statistics was about 2 hours. Therefore during an isothermal run a few spectra could be taken before the onset of crystallization, i.e., during the structural relaxation process, and the crystallization process could be followed accurately. Also at several stages of the transformation, samples were cooled down to room temperature to do x-ray-diffraction and optical-microscopy measurements.

## II. PREPARATION AND CHARACTERIZATION OF THE AMORPHOUS ALLOYS

The roller-quenched (RQ) $Fe_{80}B_{20}$ was prepared starting from 99.999%-pure Fe powder and crystalline B powder of 99.7-wt% purity. The as-quenched ribbons had a thickness of $20 \pm 2$ $\mu$m and a width of about 1 mm. The purity of the Allied Chemical Metglas (MG 2605) $Fe_{80}B_{20}$ was not specified. These ribbons were $37 \pm 1$ $\mu$m thick. The B concentration of both alloys was checked to be $20 \pm 1$ at.%. This was done by crystallizing samples at high temperature

 ©1979 The American Physical Society

(~1000 K) into the equilibrium crystalline phases $\alpha$-Fe and $Fe_2B$. Then the relative amounts of both phases in the room-temperature Mössbauer spectra could be determined which gives directly the mean B concentration, assuming that no other elements than Fe and B are present and equal recoil-free fractions of the two phases.

The two sides of the MG 2605 ribbons have a different appearance due to the method of preparation: the side which has been in contact with the metallic substrate is dull, the opposite (free) side is shiny. The two sides of the RQ $Fe_{80}B_{20}$ ribbons are indistinguishable since they were quenched in a symmetric way. X-ray diffraction (Cu K$\alpha$) shows no differences between the two kinds of as-quenched ribbons, i.e., the widths of the broad x-ray bands are equal and there are no sharp crystalline peaks. Also the dull and shiny side of MG 2605 show similar diffraction patterns. Using differential scanning calorimetry (Perkin-Elmer, DSC-1B) at a scanning rate of 32 K/min, we determined the temperature for the onset of crystallization, $T_x$. For MG 2605 $T_x = 696 \pm 2$ K and for RQ $Fe_{80}B_{20}$ $T_x = 692 \pm 2$ K. Values of $T_x$ for MG 2605 reported in the literature[8–11] range from 663 to 721 K. This large spread arises at least partly from the different scanning-rates used. For $Fe_{80}B_{20}$ quenched with the twin-roller method Fukamichi *et al.*[12] reported, without giving the scanning rate, a value of $T_x = 690$ K.

## III. RESULTS AND DISCUSSION

The amorphous to crystalline transformation was followed at four different temperatures for each of the two $Fe_{80}B_{20}$ alloys. These temperaturers were 601.0, 611.2, 621.2, and 631.5 K for MG 2605 and 581.7, 594.5, 612.2, and 625 K for RQ $Fe_{80}B_{20}$. This temperature range is 60–100 K below the crystallization temperature $T_x$ of the glasses and rather narrow (30–40 K) because of the time necessary to collect a Mössbauer spectrum. Below we first give the analysis of the crystallized alloys. Then we discuss the general characteristics of the transformation including the observed changes in the Mössbauer recoil-free fraction. Finally we turn to the kinetics of the transformation and the homogeneity of the alloys where, in contrast to the other topics just mentioned, differences between the two kinds of $Fe_{80}B_{20}$ alloys will appear.

### A. Analysis of the crystallization products

The fully crystallized alloys contain two phases: $\alpha$-Fe and the nonequilibrium[13] $Fe_3B$ compound. The B concentration of this compound was $25 \pm 1$ at.% as determined from the area ratio of the $\alpha$-Fe and $Fe_3B$ parts of the room-temperature Mössbauer spectra. The structure of the $Fe_3B$ compound was determined with x-ray diffraction. It is tetragonal with $a = 8.61$ Å, $c = 4.30$ Å, and eight units of $Fe_3B$ per primitive cell, in agreement with other authors.[14,16] As was first pointed out by Herold and Köster[15] these values of the lattice parameters are equal to those given by Rundquist[17] for the tetragonal structure of $Fe_3P_{1-x}B_x$ (for $x$ up to 0.95) when extrapolated to $Fe_3B$. There are three different crystallographic sites for the Fe atoms in this tetragonal $Fe_3B$ structure. This is in agreement with the Mössbauer spectrum of $\alpha$-Fe + $Fe_3B$ [Fig. 1(c)], which shows three different hyperfine fields for the $Fe_3B$ phase. It is worthwhile to remark that we never did find the postulated orthorhombic (isostructural to cementite) form of $Fe_3B$,[18] in contrast with Chien,[19] who only found this

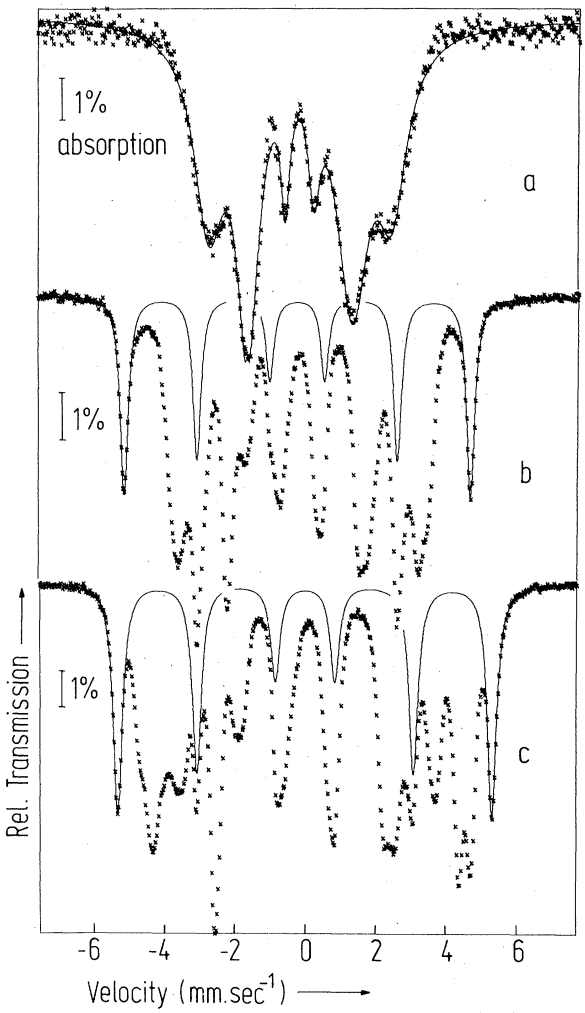


FIG. 1. Mössbauer spectra of $Fe_{80}B_{20}$ MG 2605. (a) At 601 K before crystallization occurs. (b) At 601 K after complete crystallization into $\alpha$-Fe and $Fe_3B$. The six-line pattern drawn belongs to $\alpha$-Fe and was fitted to the outer two lines only. (c) The same state as (b) but at room temperature.

orthorhombic form, together with $\alpha$-Fe, in fully crystallized samples of $Fe_{80}B_{20}$. We think that his result is rather unlikely because of the following reasons. The room-temperature Mössbauer spectra of $Fe_{80}B_{20}$ crystallized into $\alpha$-Fe + $Fe_3B$ as measured by Chien,[19] by us [Fig. 1(c)], and by others[20] clearly show (at least) three distinct hyperfine fields for the $Fe_3B$ phase. This is what we would expect, as explained before, for the tetragonal structure but not for the orthorhombic cementite-type of structure. In the latter there are only two slightly different positions for the Fe atoms. So we expect only two not very different hyperfine fields in the Mössbauer spectrum. Indeed, the Mössbauer spectra of $Fe_3C$ (Ref. 21) and of the borocarbides (also orthorhombic) $Fe_3B_xC_{1-x}$,[22] up to $x=0.54$, show only one hyperfine field with somewhat broadened lines for the higher B concentrations. It is also of importance to note that $Fe_2B$, which is the equilibrium compound,[13] was never present in the fully crystallized samples within the narrow temperature range (580–630 K) investigated by us. A transformation of ($\alpha$-Fe + $Fe_3B$) to ($\alpha$-Fe + $Fe_2B$) was observed only when the temperature was raised considerably above our range of isothermal annealing temperatures, e.g., after a few hours at 900 K. This result is again rather different from that of Chien,[19] who observed complete crystallization at 644 K, after preannealing the sample by recording Mössbauer spectra at lower temperature, into $\alpha$-Fe and $Fe_2B$ only. Chien also states that $Fe_3B$ does not appear at any stage of the process when the samples were crystallized in the way described above. When however crystallization into $Fe_2B$ and $\alpha$-Fe prevails over crystallization into $Fe_3B$ (which is nearer to the initial composition) and $\alpha$-Fe, this suggests strongly that nuclei of the $Fe_2B$ phase were already present in the amorphous matrix.

### B. Mössbauer measurements during the amorphous to crystalline transformation

From the sequence of Mössbauer spectra recorded during an isothermal run some characteristic features appear. During the first period of each isothermal run no sharp peaks corresponding to crystalline phases can be detected in the Mössbauer spectra, i.e., the alloy remains amorphous. These spectra, one of which is shown in Fig. 1(a), show the broad six-line pattern, characteristic for the amorphous state. The positions, the widths and the relative intensities of the lines do not change during this first part of the transformation. The presence of the crystalline $\alpha$-Fe and $Fe_3B$ phases can first be detected when their volume fraction is about 0.02 for the lowest, and 0.05 for the highest annealing temperature. The final spectrum at temperature of $\alpha$-Fe + $Fe_3B$ is shown in Fig. 1(b). The two outer lines of $\alpha$-Fe were fitted, the other four $\alpha$-Fe lines were calculated and are shown for convenience. From a comparison of Fig. 1(a) with Fig. 1(b) it is clear that the outer two lines of the $\alpha$-Fe six-line pattern are well separated from the amorphous and the $Fe_3B$ spectrum. This makes it possible to follow the kinetics of the transformation.

### C. Change of the recoil-free fraction

We have determined the relative values of the Mössbauer recoil-free fraction (rff) as a function of time during the amorphous to crystalline transformation. The rff or $f$-factor can be expressed as[23]

$$f=\exp(-4\pi\langle x^2\rangle/\lambda^2)\ , \tag{1}$$

where $\lambda$ is the $\gamma$-ray wavelength and $\langle x^2\rangle$ is the component of the mean-square vibrational amplitude of the nucleus ($^{57}$Fe in our case) in the direction of the $\gamma$ ray. Both the value and the temperature dependence of the rff reflect the state of the lattice. Indeed, for amorphous compared with crystalline $Sn_{1-x}Cu_x$ ($x=0.10$–$0.18$) alloys, a large difference in rff of the $^{119}$Sn nuclei was found, due to a lower Debye temperature of the amorphous phase.[24] It may be noted that the rff of the $^{119}$Sn nuclei is more sensitive to lattice changes than that of the $^{57}$Fe nuclei.[25] However no similar measurements on rff changes in liquid-quenched metallic glasses have been done to

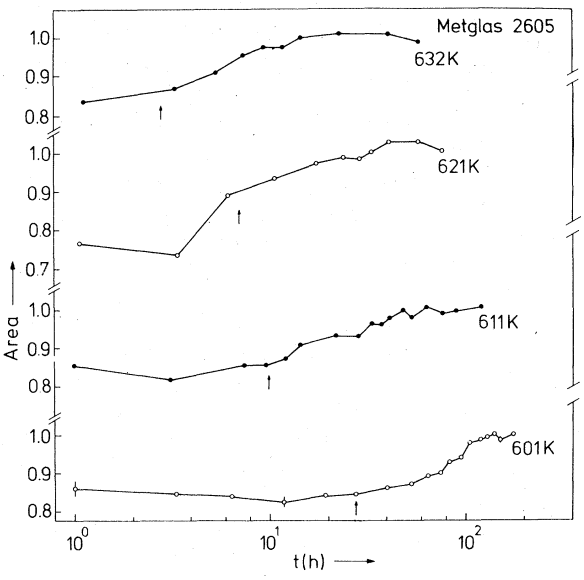


FIG. 2. Relative recoil-free fraction change during the isothermal amorphous to crystalline transformation. The data points are connected by straight lines. Representative experimental errors are shown with the 601-K data points. The arrows indicate the onset of the crystallization process.

our knowledge. For the isothermal transformation of MG 2605 $Fe_{80}B_{20}$, the area of the spectra, arbitrarily normalized to the final value for the fully crystallized alloy is plotted in Fig. 2 as a function of time. The same behavior was found for the RQ $Fe_{80}B_{20}$. This area is proportional to the rff though the relationship is not linear (due to saturation effects) if the absorber is thick as in the present case.[23] The arrows in Fig. 2 correspond to a crystallized fraction of 0.05, so they indicate roughly the onset of crystallization. The area remains constant during the structural relaxation process, before the onset of crystallization, and increases by about 15% during crystallization. Saturation effects are more important in the crystalline than in the amorphous phase because of the higher relative absorption in the former case. Thus the rff of the crystalline phase is at least 15% higher than that of the amorphous phase. This implies that on the average the Fe atoms are more firmly bound in the crystalline than in the amorphous state.

### D. Kinetics of the transformation and homogeneity of the alloys

The amount of crystallized $\alpha$-Fe can be obtained by fitting the two outer Mössbauer lines (1 and 6) of the $\alpha$-Fe sextet. $x_{Fe}(t)$ will denote the intensity of these lines at time $t$ divided by the final value, corresponding to the fully crystalline state. We will assume that this normalized $\alpha$-Fe fraction $x_{Fe}(t)$ is equal to the total volume fraction $x(t)$ of the two crystalline phases, i.e., that the $\alpha$-Fe to $Fe_3B$ ratio is constant during the transformation. This assumption will be justified later. The fraction $x(t)$ can be analyzed in terms of the Johnson-Mehl-Avrami equation[26]

$$x(t) = 1 - \exp[-(kt)^n] \,. \tag{2}$$

In this equation $k$ is a temperature-dependent constant and the value of the exponent $n$ is determined by the characteristics of the nucleation-and-growth process. From Eq. (2) it follows that a log-log plot of $\ln[1/(1-x)]$ versus time gives a straight line with slope $n$. Such plots for MG 2605 (Fig. 3) and RQ $Fe_{80}B_{20}$ (Fig. 4) show two sets of straight lines with different slopes: $n = 2.4 \pm 0.2$ $(0.10 \leq x \leq 0.80)$ and $n = 1.3 \pm 0.1$ $(0.05 \leq x \leq 0.90)$, respectively. We note that for MG 2605 (Fig. 3) the last part of the plot ($x \gtrsim 0.8$) has a lower slope ($\sim 1$). We will discuss these features of the time dependence of the transformation in more detail together with the results obtained by optical microscopy.

The activation energy for the crystallization process $E_A$, was determined from the time $t_x$, corresponding to a crystalline fraction $x$, using the Arrhenius equa-

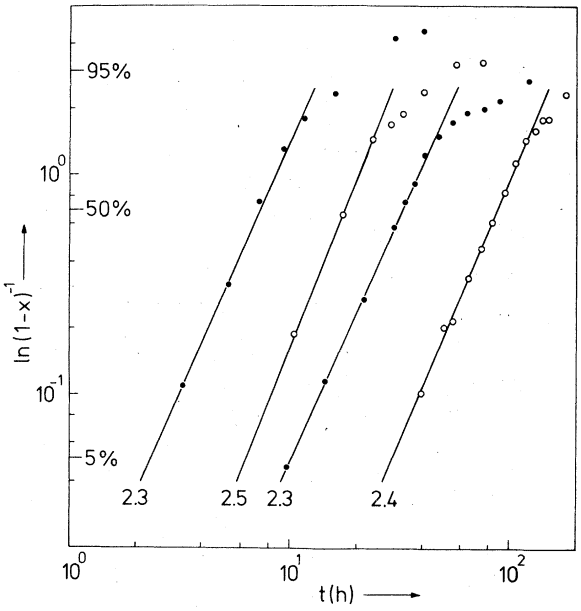


FIG. 3. Crystallized fraction ($x$) of $Fe_{80}B_{20}$ MG 2605 plotted as $\ln(1-x)^{-1}$ vs time on log-log scale [see Eq. (2)] at, from the left to the right, 632.5, 621.2, 611.2, and 601 K. The lines drawn are a fit to Eq. (2) for $x \leq 0.8$. Values of the exponent $n$ in this equation are indicated.

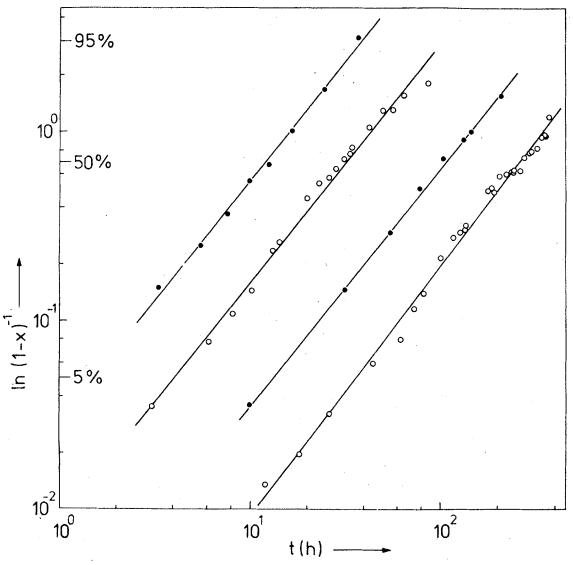


FIG. 4. Crystallized fraction ($x$) of RQ $Fe_{80}B_{20}$; plotted like Fig. 3, at, from the left to the right, 625.0, 612.2, 594.5, and 581.7 K. The lines drawn are a fit to Eq. (2). The slopes are equal: $n = 1.3 \pm 0.1$.

tion for a thermally activated process[27]

$$t_x = k_0^{-1} \exp\left(\frac{E_A}{k_B T}\right) , \quad (3)$$

where $k_0$ is a frequency factor and $k_B$ is the Boltzmann constant. In Fig. 5 the Arrhenius plots (for $t_{0.5}$) are shown. For MG 2605 $E_A = 2.5 \pm 0.2$ eV/atom and for RQ $Fe_{80}B_{20}$ $E_A = 2.2 \pm 0.2$ eV/atom independent of $x$ ($0.1 < x < 0.8$). For MG 2605 we found the same activation energy ($2.5 \pm 0.1$ eV/atom) in the 690–740 range from differential scanning calorimetry (DSC) measurements (peak-shift method[28]). This indicates that there is no change in the crystallization mechanism between 600 and 740 K. The kinetic parameters $n$ [Eq. (2)], and $E_A$ [Eq. (3)] are collected in Table I together with some reported values. All the activation energies are in reasonable agreement with each other.

Complementary information about the crystallization process was obtained from optical microscopy (OM) and x-ray-diffraction measurements carried out at room temperature on samples with different crystalline fractions $x$. With x-ray diffraction (Cu K$\alpha$, reflection geometry) we observed a large difference in the crystallization behavior of the two sides of the MG 2605 ribbons. For as-quenched ribbons both sides are similar [Fig. 6(a)]. However, after annealing to a crystalline fraction of about 0.8, the substrate side of the ribbons is still mainly amorphous [Fig. 6(b)] whereas the free side is almost fully crystallized

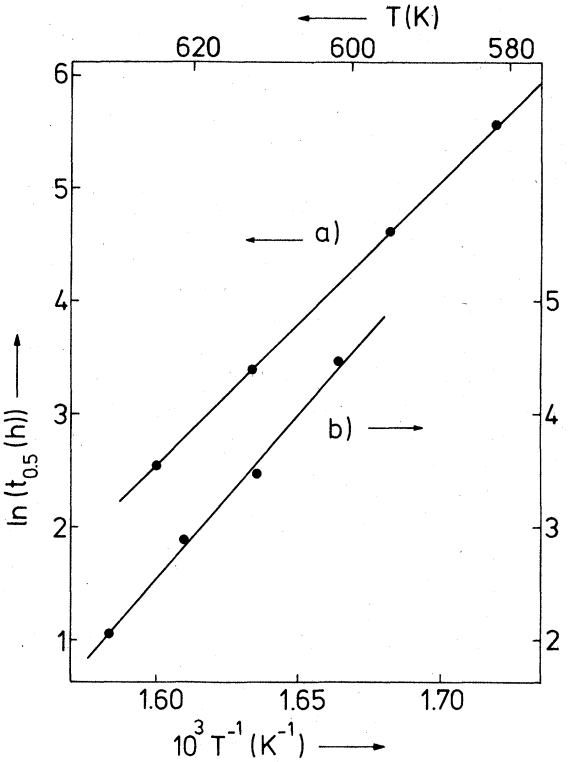


FIG. 5. Arrhenius plot for (a) $Fe_{80}B_{20}$ RQ (twin-roller), $E_A = 2.2 \pm 0.2$ eV/atom and (b) $Fe_{80}B_{20}$ MG 2605, $E_A = 2.5 \pm 0.2$ eV/atom.

TABLE I. Kinetic parameters $n$ [Eq. (2)] and $E_A$ [Eq. (3)] for the crystallization of $Fe_{80}B_{20}$.

| | $n$ | $E_A$ (eV/atom) | Temp. range | Ref. |
|---|---|---|---|---|
| $Fe_{80}B_{20}$ MG 2605 | $2.6 \pm 0.2$[a] | $2.5 \pm 0.2$[b] | 600–630 K | present study |
| | | $2.5 \pm 0.1$[c] | 690–740 K | present study |
| | $2.2 \pm 0.2$[c] | $2.5 \pm 0.05$[c] | | 10 |
| | | 2.66[d] | 660–705 K | 8 |
| | | 2.02[e] | 560–670 K | 30 |
| | | 2.1[f] | 570–720 K | 14 |
| | | 2.1[g] | 590–680 K | 11 |
| $Fe_{80}B_{20}$ RQ (twin-roller quenched) | $1.3 \pm 0.1$ | $2.2 \pm 0.2$[b] | 580–625 K | present study |
| $Fe_{80}B_{20}$ (spinning-wheel quenched) | | $2.45 \pm 0.1$[h] | ~680–740 K | 35 |

[a]Value obtained from the homogeneous part A (see Fig. 7) of the ribbon cross section.
[b]Independent of the crystalline fraction $x$ ($0.1 < x < 0.9$).
[c]From dynamic calorimetric measurement.
[d]Applying to $x = 0.5$, obtained from isothermal calorimetric measurements.
[e]Applying to the growth process, obtained from transmission-electron microscopy (TEM).
[f]Applying to the nucleation process, obtained from TEM.
[g]Applying to the onset of crystallization, obtained from coercive-force changes and isothermal calorimetric measurements.
[h]Applying both to the onset of and subsequent crystallization, obtained from dynamic calorimetric measurements.

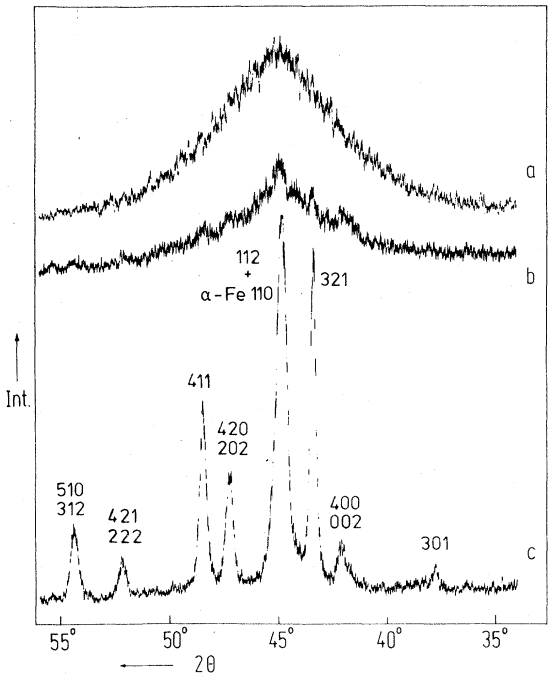


FIG. 6. X-ray diffraction patterns (Cu K$\alpha$; reflection geometry) of $Fe_{80}B_{20}$ MG 2605. (a) As-quenched (vertical scale $\times 2$), (b) substrate (dull) side of ribbons after 40 h at 611 K, and (c) free (shiny) side of ribbons after 40 h at 611 K. The Miller indices of the reflections of the $\alpha$-Fe and $Fe_3B$ (tetragonal) crystalline phases are indicated.

[Fig. 6(c)]. We remark that only a layer of about 1 $\mu$m near to the surface contributes to the diffracted intensity. For samples annealed further, to $x = 1$ as determined with Mössbauer-effect spectroscopy, the substrate side was also fully crystallized into $\alpha$-Fe and $Fe_3B$ and the x-ray-diffraction data were qualitatively equal to those of the free side of the ribbons. The micrographs of the cross section of partially crystallized ribbons of MG 2605 and RQ $Fe_{80}B_{20}$ are schematically represented in Fig. 7. For MG 2605 the substrate side ($B$ in Fig. 7) does not contain crystalline material, in agreement with the x-ray-diffraction result, and is $5 \pm 1$ $\mu$m thick, i.e., 10% to 15% of the total thickness. The series of micrographs further shows that this substrate side crystallizes only after complete crystallization of the main part ($A$ in Fig. 7) of the ribbon cross section and takes place probably by parallel displacement of the boundary plane between $A$ and $B$ into $B$. This explains the change of slope of the Avrami plot (Fig. 3) for MG 2605 because we may conclude now that the first part ($x \lesssim 0.8$) corresponds to the crystallization of part $A$ of the ribbons. Here the growth takes place in three dimensions as can be seen from the ellipsoidal shape

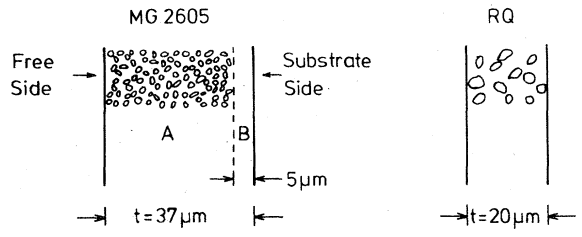


FIG. 7. Schematic representation of optical micrographs of the cross section of partially crystallized ribbons of MG 2605 and RQ $Fe_{80}B_{20}$ ($t$ is the thickness). The distribution of crystalline spherulites is random and homogeneous in the RQ ribbons and in the main part $A$ of the MG 2605 ribbons. However the substrate side $B$ of MG 2605 starts to crystallize only after complete crystallization of part $A$.

of the crystalline "spherulites". The last part of the plot (Fig. 3) corresponds to the crystallization of part $B$ and according to the theory[26] a lower value for the exponent $n$ of Eq. (2) is expected when the growth process is of lower dimensionality. During continuous heating in a DSC we observed a shoulder on the high-temperature side of the main crystallization peak. This shoulder clearly corresponds to part $B$ of the ribbon because it disappeared when a surface layer was removed from the substrate side. From our data we could not determine the cause of the higher resistance against crystallization of the substrate side of the MG 2605 ribbons. That it is not only an artefact of our MG 2605 samples follows from the fact that two other groups of workers[9,14] did also observe the same type of inhomogeneity. OM did not reveal such an inhomogeneity for the RQ $Fe_{80}B_{20}$.

As indicated in Fig. 7 for the RQ $Fe_{80}B_{20}$, as for the main part ($A$) of the MG 2605, the distribution of crystalline spherulites was random and homogeneous in the whole cross section of the ribbons. This allows us to determine quantitatively the (total) fraction $x$ of crystalline material from the micrographs using the point-counting method of Hilliard and Cahn.[29] The normalized $\alpha$-Fe fraction $x_{Fe}$ as determined with Mössbauer-effect spectroscopy (MES), is plotted in Fig. 8 versus the total crystalline fraction $x$ from OM, where we note that the values for MG 2605 apply to the homogeneous part of the ribbons and the corresponding $x_{Fe}$ values have been corrected in this sense. The data points are close to the straight line indicating a linear relationship, which justifies our assumption made earlier that the $\alpha$-Fe to $Fe_3B$ ratio remains constant during the crystallization process.

### E. Crystallization process

The linear relation observed between the crystalline $\alpha$-Fe fraction and the total crystalline fraction supports the description of the crystallization process of amorphous $Fe_{80}B_{20}$ as a eutectic reaction. This was also concluded from electron microscopy[14,30] results. A different type of crystallization process, namely a two-step process, has frequently been observed[10,12,30–32] for amorphous Fe-B alloys with a B concentration of less than about 17% and was also proposed for higher (up to 25 at.%) B concentrations.[10] The first step is precipitation of $\alpha$-Fe together with a shift of the B concentratioin of the matrix which remains amorphous until 25-at.% B content, and the second step is the polymorphous crystallization of this matrix into $Fe_3B$. Kemény *et al.*[10] did determine both the normalized $\alpha$-Fe fraction $x_{Fe}$ (with MES) and the total crystalline fraction $x$ (with differential scanning calorimetry) for $Fe_{83}B_{17}$, like we did for $Fe_{80}B_{20}$. Their data (see Fig. 8) show the saturation of $x_{Fe}$ expected for the two-step process, and they propose that this two-step process will also occur for Fe-B alloys with B concentrations up to 25 at.%. This is clearly contradicted by the linear relation found by us for $Fe_{80}B_{20}$ (Fig. 8).

We can now say something more about the interpretation of the measured kinetic exponent $n$ of Eq. (2). Experimentally we found for MG 2605 $n = 2.4 \pm 0.2$, which increases slightly to $n = 2.6 \pm 0.2$ when we correct properly to describe only the homogeneous part $A$ (see Fig. 7) of the ribbon, and for RQ $Fe_{80}B_{20}$ $n = 1.3 \pm 0.1$. According to the theory, for the eutectic reaction the conditions for a linear growth law are fulfilled, essentially because there is no change in mean composition across the amorphous-crystalline interface, so there is no need for long-range diffusion (which would give a parabolic growth law) in the amorphous phase. A detailed discussion of the possible processes and the corresponding kinetic exponents $n$ can be found elsewhere.[26] Linear growth in each dimension was actually found with transmission-electron microscopy (TEM) for MG 2605 (Ref. 30) and leads to an exponent $n = 3$ for three dimensional growth, apart from the additional contribution of the nucleation. This nucleation contribution is zero only when there is no nucleation, i.e., growth of a fixed number of pre-existing nuclei (then $n = 3$), and, e.g., equal to 1 for a constant nucleation rate (then $n = 4$). The experimental values $n = 2.6$(MG 2605) and $n = 1.3$ (RQ) are closest to the theoretical value $n = 3$, but they are rather low. The agreement between theory and experiment is only satisfactory for MG 2605. We think that these low-experimental values indicate strongly that nucleation is very difficult at relatively low temperatures and that the crystallization takes place only by growth of nuclei already present in the amorphous matrix. These nuclei were formed during the quench from the liquid. We will give some more arguments supporting this point of view.

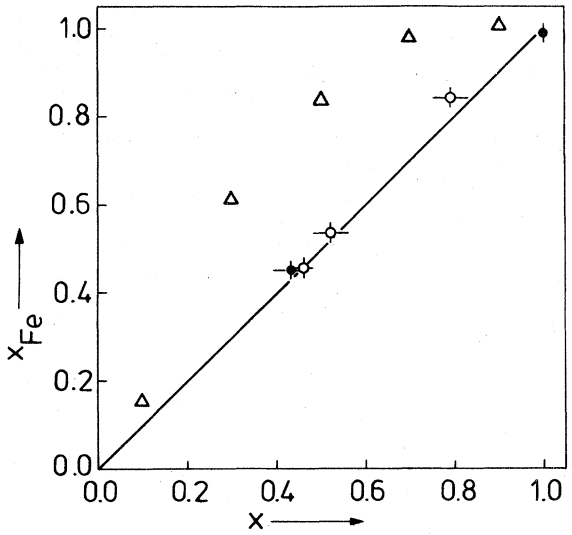


FIG. 8. Normalized $\alpha$-Fe fraction $x_{Fe}$, obtained from Mössbauer-effect spectroscopy, versus total crystalline fraction $x$, obtained from optical microscopy for MG 2605 $Fe_{80}B_{20}$ (open circles) and RQ $Fe_{80}B_{20}$ (full circles). The straight line corresponds to a linear relationship. Also shown are data taken from Ref. 10 for $Fe_{83}B_{17}$ (triangles) where the values for the total fraction $x$ (horizontal axis) were obtained from calorimetric measurements.

First, it has been shown[33] that the critical quenching rate necessary to prevent nucleation, is considerably higher (several orders of magnitude) than the critical quenching rate necessary to prevent crystallization. Since $Fe_{80}B_{20}$ is not an easy glass former it is likely that during the quench nuclei are formed. Further there is some experimental evidence[34] that the quenching rate is higher for twin-roller quenching compared with quenching on the outer surface of a rotating wheel (i.e., the way the MG 2605 ribbons are produced), because of a better heat transfer between liquid and substrate in the former case. This is qualitatively in agreement with our OM result that the number of crystalline spherulites per unit volume is a factor of 10 to 100 greater for MG 2605 than for RQ $Fe_{80}B_{20}$ (after annealing to equal crystalline fractions at equal temperatures), if there is only growth of a fixed number of pre-existing nuclei. Finally, from activation-energy determinations, there is no indication for a separate nucleation stage. In fact, we observed that the activation energy (for $0.1 < x < 0.8$) does not depend on the crystalline fraction $x$. Also with TEM[14] and DSC[35] the activation energy for the very onset of crystallization was found to be equal to that of the subsequent crystallization process (see also the data in Table I). This is of course what we expect, though it is no proof of it, when there is no nucleation.

## ACKNOWLEDGMENTS

We would like to thank Ir. A. L. Mulder (Department of Technical Physics, Utrecht) for quenching the $Fe_{80}B_{20}$ with the twin-roller technique. Mr. H. Bron (Physical Metallurgy Laboratory, Groningen) for the optical microscopy work, and Professor W. G. Perdok for his help with the intepretation of the x-ray-diffraction data. This work is part of the research program of the "Stichting voor Fundamenteel Onderzoek der Materie" [Foundation for Fundamental Research on Matter (FOM)] and was made possible by financial support from the "Nederlandse Organisatie voor Zuiver Wetenschappelijk Onderzoek" (Netherlands Organization for the Advancement of Pure Research ZWO).

[1]H. S. Chen and D. E. Polk, J. Non-Cryst. Solids 15, 174 (1974).
[2]G. C. Chi, H. S. Chen, and C. E. Miller, J. Appl. Phys. 49, 1715 (1978).
[3]B. G. Lewis and H. A. Davies, in *The Structure of Non-Crystalline Materials,* edited by P. H. Gaskell (Taylor and Francis, London, 1977), p. 89.
[4]H. S. Chen, Scr. Metall. 11, 367 (1977).
[5]H. H. Liebermann, C. D. Graham, Jr., and P. J. Flanders, IEEE Trans. Magn. 13, 1541 (1977).
[6]T. Egami and T. Ichikawa, Mater. Sci. Eng. 32, 293 (1978).
[7]H. S. Chen and C. E. Miller, Rev. Sci. Instrum. 41, 1237 (1970).
[8]L. A. Davis, R. Ray, C.-P. Chou, and R. C. O'Handley, Scr. Metall. 10, 541 (1976).
[9]A. L. Greer and J. A. Leake, in *Rapidly Quenched Metals III,* edited by B. Cantor (The Metals Society, London, 1978), Vol. 1, p. 299.
[10]T. Kemény, I. Vincze, B. Fogarassy, and S. Arajs, in Ref. 9, p. 291.
[11]F. E. Luborsky, Mater. Sci. Eng. 28, 139 (1977).
[12]K. Fukamichi, M. Kikuchi, S. Arakawa, and T. Masumoto, Solid State Commun. 23, 955 (1977).
[13]M. Hansen, *Constitution of Binary Alloys* (McGraw-Hill, New York, 1958).
[14]U. Köster and U. Herold, Scr. Metall. 12, 75 (1978).
[15]U. Herold and U. Köster, Z. Metallkd. 69, 326 (1978).
[16]J. L. Walter, S. F. Bartram, and R. R. Russell, Metall. Trans. A 9, 803 (1978).
[17]S. Rundquist, Acta Chem. Scand. 16, 1 (1962).
[18]R. Fruchart and A. Michel, Mem. Soc. Chim. Fr. 422 (1959).
[19]C. L. Chien, Phys. Rev. B 18, 1003 (1978).
[20]H. Franke, U. Herold, U. Köster, and M. Rosenberg, in *Rapidly Quenched Metals III,* edited by B. Cantor (The Metals Society, London, 1978), Vol. 1, p. 155.
[21]M. Ron, H. Schechter, A. A. Hirsch, and S. Niedzwiedz, Phys. Lett. 20, 481 (1966).
[22]H. Bernas, I. A. Campbell, and R. Fruchart, J. Phys. Chem. Solids 28, 17 (1967).
[23]N. N. Greenwood and T. C. Gibb, *Mossbauer Spectroscopy* (Chapman and Hall, London, 1971).
[24]J. Bolz and F. Pobell, Z. Phys. B 20, 95 (1975).
[25]V. I. Goldanskii and R. H. Herber, *Chemical Applications of Mossbauer Spectroscopy* (Academic, New York, 1968), p. 326.
[26]J. W. Christian, *The Theory of Transformations in Metals and Alloys,* second ed. (Pergamon, Oxford, 1975), Part I.
[27]J. Burke, *The Kinetics of Phase Transformations in Metals* (London, Pergamon, 1965).
[28]J. F. Nicholas, Aust. J. Phys. 9, 425 (1956).
[29]J. E. Hilliard and J. W. Cahn, Trans. AIME 221, 344 (1961).
[30]U. Herold and U. Köster, in *Rapidly Quenched Metals III,* edited by B. Cantor (The Metals Society, London, 1978), Vol. 1, p. 281.
[31]We did observe with MES (unpublished results) the two-step process in $Fe_{82.5}B_{17.5}$ and also in $Fe_{85}B_{15}$ where only the first of the two steps takes place at lower temperatures.
[32]F. E. Luborsky, H. H. Liebermann, J. J. Becker, and J. L. Walter, in *Rapidly Quenched Metals III,* edited by B. Cantor (The Metals Society, London, 1978), Vol. 2, p. 188.
[33]H. A. Davies, Ref. 32, Vol. 1, p. 1.
[34]See Ref. 33 and references therein.
[35]F. E. Luborsky and H. H. Liebermann, Appl. Phys. Lett. 33, 233 (1978).